

# Sulfurized Polypropylene as Low-Cost Cathode Material for High-Capacity Lithium-Sulfur Batteries

Qian Du,<sup>[a]</sup> Mathis Benedikter,<sup>[a]</sup> Kathrin Küster,<sup>[b]</sup> Tolga Acartürk,<sup>[b]</sup> Ulrich Starke,<sup>[b]</sup> Jean-Louis Hoslauer,<sup>[c]</sup> Thomas Schleid,<sup>[c]</sup> and Michael R. Buchmeiser<sup>\*[a, d]</sup>

Among 'beyond lithium ion' energy storage, lithium sulfur (Li-S) batteries are one of the most promising technologies, as a result of the potential for high theoretical energy capacity at low cost. A key obstacle in exploiting the vast potential of Li-S batteries is the formation of soluble polysulfide species. Here, we report sulfurized polypropylene (S/PP-500) synthesized in one-step by reacting polypropylene (PP) with sulfur as a new polysulfide shuttle-free cathode material for Li-S batteries. It

exhibits a reversible capacity as high as 1000 mAh/g<sub>sulfur</sub> at 0.1 C and a sulfur loading of up to 68 wt%, which in turn allows for high sulfur loadings up to 47% in the final cathode. The low-cost starting materials together with the simple synthetic procedure and the good electrochemical performance in combination with a commercially available electrolyte make the S/PP-500 a very promising cathode material for Li-S batteries.

## Introduction

Batteries are essential to our modern society. They are ubiquitous in our daily life, e.g., in many electronic devices or electric vehicles. Furthermore, they are part of the green energy transition, making the development of batteries more important than ever. The global necessity for battery-based energy storage has been growing exponentially in recent years.<sup>[1]</sup> The limited theoretical capacity of lithium-ion batteries poses a major challenge in meeting the high demand for energy storage.<sup>[2]</sup> Therefore, substantial research has been devoted to novel, high-energy density, environmentally friendly next-generation batteries.<sup>[3]</sup> Among other batteries, lithium sulfur (Li-S) batteries are considered one of the most promising 'beyond Li-ion' batteries for the following reasons: (1) sulfur is non-toxic, inexpensive and highly abundant and (2) sulfur has a high theoretical discharge capacity of up to 1672 mAh/g<sub>sulfur</sub>. Consequently, Li-S batteries could substantially reduce the cost of raw materials and offer high energy density.<sup>[4]</sup> Nonethe-

less, the widespread practical application of Li-S batteries is still hampered by several challenges such as (1) poor conductivity of S<sub>8</sub> ( $5 \times 10^{-30}$  S cm<sup>-1</sup> at 25 °C) and Li<sub>2</sub>S, (2) a large volume change during cycling, and (3) the formation of polysulfides (Li<sub>2</sub>S<sub>x</sub>, 1 < x ≤ 8) as intermediates during cycling. Once the polysulfides are formed, they can dissolve in the electrolyte and shuttle from the cathode to the anode, where they react with lithium to form Li<sub>2</sub>S. As a result, both energy density and rechargeability are permanently reduced. This phenomenon is referred to as polysulfide-shuttle and is one of the major challenges in Li-S batteries.<sup>[5-8]</sup>


Different approaches have been designed to tackle this issue, which can be classified into a modification of the cathode, the separator and the interlayer.<sup>[9]</sup> All these modifications are designed to suppress the polysulfide shuttle via physical confinement, chemisorption or catalytic effects.<sup>[10]</sup> The corresponding modified cathode materials, such as porous conductive carbon matrices,<sup>[11-16]</sup> metal-organic frameworks (MOFs),<sup>[9]</sup> and transition metal oxides,<sup>[17]</sup> are the most prominent with which the challenges in Li-S batteries are tackled.<sup>[11,12,14-16]</sup> A conductive carbon matrix can thereby increase the overall conductivity and buffer the volume change during cycling. Microporous or mesoporous materials can confine polysulfides inside the pores, which suppress the polysulfide shuttle to a certain extent.<sup>[13]</sup> However, porous carbon materials commonly require rather complicated synthetic processes and sulfur loadings are limited in order to effectively suppress the polysulfide dissolution.<sup>[7]</sup> Consequently, any large-scale production of these materials is complicated and expensive.<sup>[7]</sup> A second approach comprises the synthesis of cathode materials with sole solid phase conversion, which directly avoids the polysulfide shuttle.<sup>[18,19]</sup> Representative compounds are sulfurized poly(acrylonitrile) (SPAN),<sup>[20-25]</sup> or sulfurized carbyne,<sup>[26]</sup> alucone-coated C-S electrodes<sup>[27]</sup> and graphdiyne-like porous organic frameworks.<sup>[28]</sup> Cathode materials in this category provide high specific discharge capacity and


[a] Q. Du, M. Benedikter, Prof. M. R. Buchmeiser  
Institute of Polymer Chemistry, University of Stuttgart  
70569 Stuttgart, Germany  
E-mail: michael.buchmeiser@ipc.uni-stuttgart.de

[b] K. Küster, T. Acartürk, Prof. U. Starke  
Max Planck Institute for Solid State Research  
Heisenbergstraße 1, 70569 Stuttgart, Germany

[c] J.-L. Hoslauer, Prof. T. Schleid  
Institute of Inorganic Chemistry  
University of Stuttgart  
70569 Stuttgart, Germany

[d] Prof. M. R. Buchmeiser  
German Institutes of Textile and Fiber Research (DITF) Denkendorf  
Körschtalstraße 26, 73770 Denkendorf, Germany

 Supporting information for this article is available on the WWW under <https://doi.org/10.1002/batt.202200277>

 © 2022 The Authors. Batteries & Supercaps published by Wiley-VCH GmbH. This is an open access article under the terms of the Creative Commons Attribution License, which permits use, distribution and reproduction in any medium, provided the original work is properly cited.

stable performance owing to the absence of the polysulfide-shuttle. However, one major drawback of these materials is the low sulfur loading. SPAN has a sulfur loading lower than 45 wt%,<sup>[21–25]</sup> while the graphdiyne-like porous organic frameworks have sulfur loadings up to 56.8 wt%,<sup>[28]</sup> which is the highest for cathode materials with sole solid phase transformation. Herein, we report a sulfur-containing polymeric cathode material with sulfur loadings up to 68 wt% that can be used in polysulfide-shuttle free Li–S batteries, namely sulfurized polypropylene (S/PP-500), which is prepared via a facile one-step reaction of S<sub>8</sub> with polypropylene (PP) at 500 °C.

## Results and Discussion

### Synthesis of sulfurized PP

PP was chosen as candidate for sulfurization due to the presence of a tertiary carbon atom in every repeat unit, which can easily react with sulfur at elevated temperatures. In the course of this reaction, hydrogen is removed as H<sub>2</sub>S and sulfur is chemically bound to the polymer in form of short C–S<sub>x</sub>–C chains (1 ≤ x < 8). Accordingly, sulfurized PP (S/PP-500) can be prepared in a facile one-step vulcanization process (Figure 1)

via a reaction of PP with excess elemental sulfur at 500 °C under N<sub>2</sub>. Unreacted sulfur was then removed by Soxhlet extraction with toluene. This allowed for full removal of S<sub>8</sub> physically adsorbed to the polymer, selectively preserving the sulfur that is chemically bound to the polymer matrix. A sulfur loading of up to 68 wt% was obtained, which exceeds the loading of other cathode materials based on solid phase transformation.

### Structure of S/PP-500

To elucidate the structure of S/PP-500, it was subjected to thermogravimetric analysis-mass spectrometry (TGA-MS, Figure 2a).

A first weight loss was observed between 200 °C and 300 °C under the concomitant release of C<sub>3</sub>H<sub>3</sub> (m/z = 39) and C<sub>4</sub>H<sub>3</sub> (m/z = 51), corresponding to the decomposition of PP, while the second weight loss above 300 °C entailed the formation of the fragments HS (m/z = 33), H<sub>2</sub>S (m/z = 34), CS (m/z = 44) and CS<sub>2</sub> (m/z = 76). Formation of the HS and H<sub>2</sub>S fragments point towards a sulfur-triggered dehydrogenation while the formation of CS and CS<sub>2</sub> fragments are indicative for the decomposition of the sulfurated polymer. An SEM image of a cathode material based on S/PP-500 is shown in Figure 2b. As can be

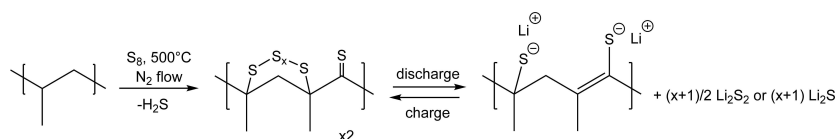


**Figure 1.** Synthesis of S/PP-500 and reversible discharging/charging of S/PP-500. (Oxidized sulfur, which was formed due to oxygen residue during the synthesis process, is not displayed).

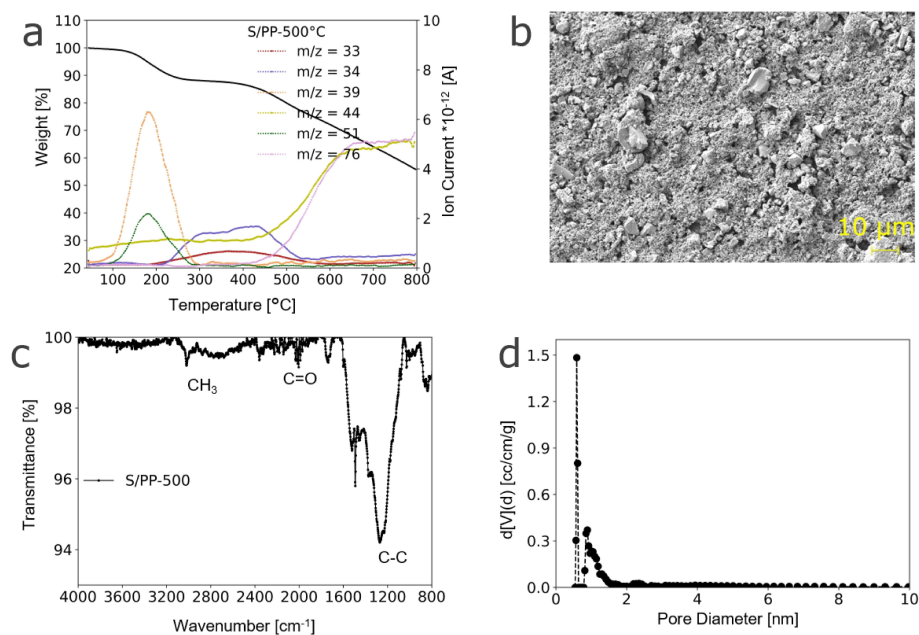


**Figure 2.** a) TGA-MS curves of S/PP-500 recorded between 45 °C and 800 °C applying a heating rate of 10 K/min and m/z values of the most prominent gaseous products (black line represents weight loss), b) SEM image of a cathode material based on 70 wt% S/PP-500, 15 wt% PVDF and 15 wt% carbon black. c) Infrared spectrum of S/PP-500. d) Pore size distribution of S/PP-500.

seen, the particle size of S/PP-500 is not uniform and varies approx. between 1 and 60  $\mu\text{m}$ . Improved particle size distribution is likely to improve the coating quality towards high electrochemical performance. The infrared spectrum of S/PP-500 is shown in Figure 2c; peaks correspond to the C–C ( $1220\text{ cm}^{-1}$ ), C=O ( $1720\text{ cm}^{-1}$ ) and C–H ( $2980\text{ cm}^{-1}$ ) vibrations.<sup>[26]</sup> It is worth mentioning that no characteristic peak corresponding to an aromatic structure was found. Therefore, no significant capacity contribution from the polymer matrix must be expected once the cutoff voltage is set  $< 1\text{ V}$ .<sup>[29]</sup> After the vulcanization process, S/PP-500 had a surface area of  $497.4\text{ m}^2/\text{g}$  and a pore size of ca.  $0.6\text{ nm}$  (Figure 2d). The porous structure of S/PP-500 can be expected to buffer volume changes during redoxing to a certain extent, which is beneficial for a long cycle life.

### ToF-SIMS, XPS and PXRD spectra

Time-of-flight secondary ion mass spectrometry (ToF-SIMS) and X-ray photoelectron spectroscopy (XPS) on pristine S/PP-500 provided further chemical insights. The ToF-SIMS spectra of a pristine S/PP-500 electrode (Figure 3a) revealed only sulfur chains not longer than  $\text{S}_4$ , which suggests that sulfur exists in the polymer backbone in form of short sulfide bridges. The S 2p and C 1s XPS spectra of a pristine S/PP-500 cathode are shown in Figure 3b,c. Two peaks located at  $162.4\text{ eV}$  and  $164.3\text{ eV}$  (Figure 3b, Table S1), which can be ascribed to the C=S S 2p<sub>3/2</sub> and C–S/S–S S 2p<sub>3/2</sub> signals, respectively, are observed. Clearly, no elemental sulfur ( $164.0\text{ eV}$ ) is detected, which indicates efficient Soxhlet extraction.<sup>[30]</sup> Instead, the XPS

spectrum confirms that sulfur is covalently bound to the polymer backbone in form of C=S and C–S bonds. (Figure 3c).

In order to determine the potential presence of any elemental sulfur in the cathode material during the redox process, X-ray powder diffraction (PXRD) patterns for a pristine cathode as well as for cathodes (discharged to  $1\text{ V}$  and  $0.45\text{ V}$ ) and fully charged to  $3\text{ V}$  were recorded (Figure 4). The patterns clearly do not indicate any detectable amounts of crystalline sulfur polymorphs such as orthorhombic or monoclinic  $\text{S}_8$  or larger  $\text{S}_x$  modifications as reported in the PDF-2 database.<sup>[31]</sup> These results are in line with ToF-SIMS and XPS analysis and further confirm that the sulfur is covalently bound to the polymer backbone, both in the pristine and fully recharged state. Moreover, it indicates that all sulfur becomes reattached to the polymer backbone in a reversible process. Interestingly, the diffraction pattern of the pristine cathode material was almost identical to the one of a cathode material discharged to  $1\text{ V}$  with only minor differences due to a different sample thickness. This suggests that discharge to  $1\text{ V}$  as the cutoff voltage is insufficient to finish the redox process in S/PP-500 (Figure 5b). While the discharged samples do not indicate the formation of any crystalline phase, additional reflections can be found in the sample that had been charged to  $3\text{ V}$ . These additional reflections could be matched to monoclinic  $\text{Li}_2\text{CO}_3$ ,<sup>[32]</sup> which has been reported to form in lithium-based batteries in the reaction with carbonate-based organic solvents.<sup>[33]</sup> To offer direct proof of the absence of long-chain polysulfides, a cell based on S/PP-500 was cycled 100 times, fully discharged to  $0.45\text{ V}$  and then submitted to ultraviolet-visible (UV-vis) spectroscopy and a visual experiment. As shown in Figure 4(b), no formation of long-chain polysulfides ( $\text{Li}_2\text{S}_x$ ,  $4 \leq x \leq 8$ ) was

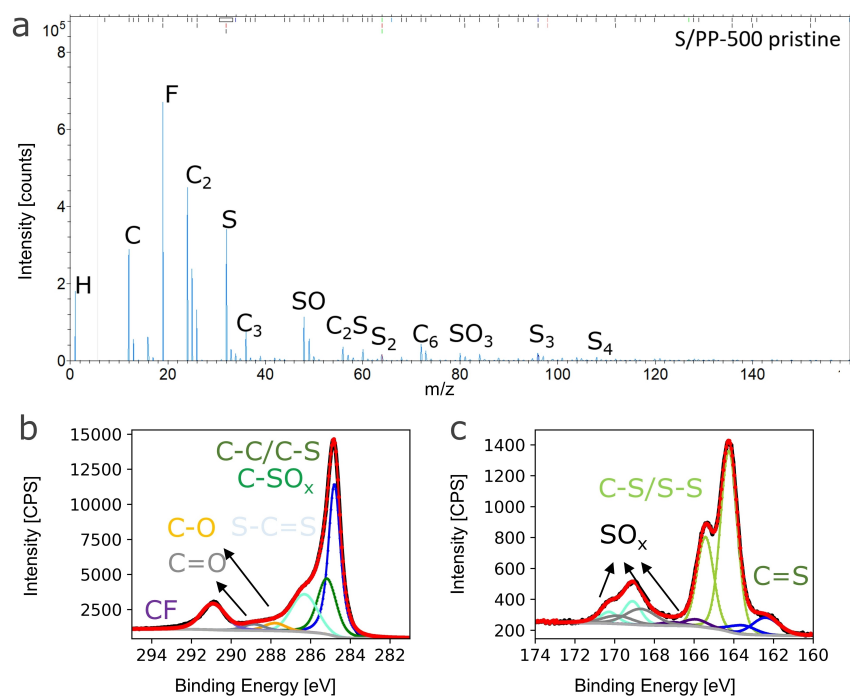


**Figure 3.** a) TOF-SIMS spectrum, b) S 2p and c) C 1s XPS spectra of a pristine S/PP-500 cathode containing 70 wt% S/PP-500 as active material with 15 wt% PVDF as binder and 15 wt% carbon black as conductive additive.

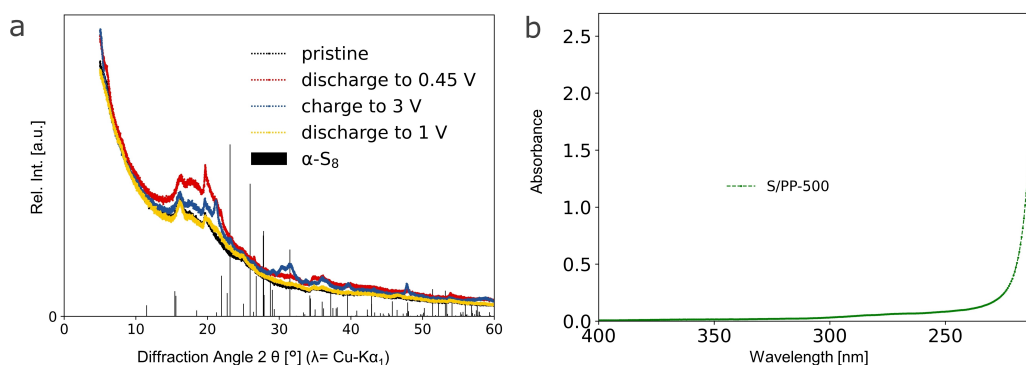


**Figure 4.** a) Stacked PXRD patterns of pristine S/PP-500 cathode material (black line), S/PP-500 cathode material discharged to 0.45 V (red line) after 100 cycles, S/PP-500 cathode material fully charged to 3 V after 100 cycles and S/PP-500 cathode material discharged to 1 V after 100 cycles. The black vertical lines represent the theoretical reflection positions of orthorhombic  $\alpha$ -S<sub>8</sub>.<sup>[35]</sup> All four samples contain 70 wt% S/PP-500, 15 wt% PVDF and 15 wt% carbon black. b) UV-vis spectrum of S/PP-500. Reference sample was LiPF<sub>6</sub> in a solution of EC: DEC at a volume ratio of 1:1.

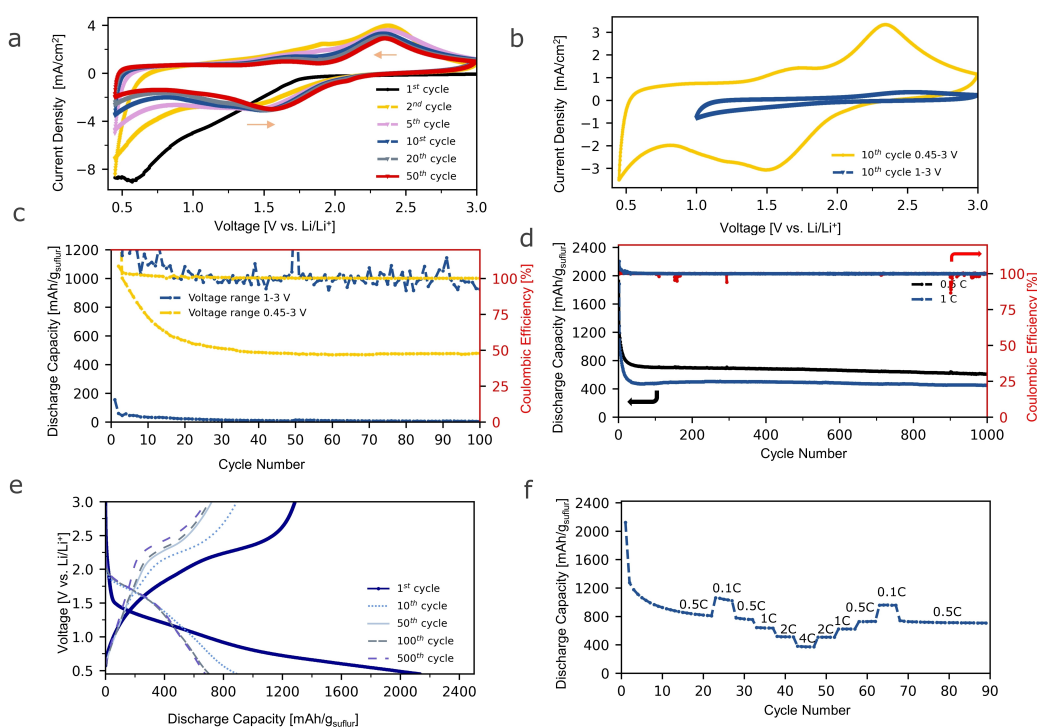


**Figure 5.** a) Cyclic voltammogram of S/PP-500 in a voltage range between 0.45 V and 3 V applying a scan rate of 1 mV/s. b) Cyclic voltammogram of S/PP-500 at a cutoff voltage of 0.45 V (yellow line) and 1 V (blue line), both at the 10<sup>th</sup> cycle applying a scan rate of 1 mV/s. c) Cycle test for S/PP-500 at a C-rate of 1 C with a cutoff voltage of 0.45 V (yellow) and 1 V (blue), respectively. d) Cycle test for S/PP-500 at a C-rate of 1 C (blue) and 0.5 C (black) at a voltage range between 0.45 and 3 V. e) Discharge profile for S/PP-500 at a C-rate of 0.5 C with a cutoff voltage of 0.45 V. f) Stress test for S/PP-500 at various C-rates with a cutoff voltage of 0.45 V.

observable. Moreover, no color change in the electrolyte was witnessed in the visual experiment. These findings further support the proposal that sulfur is covalently bound to the polymer backbone and participates in the redoxing process via a solid phase transformation. This is in line with the structure of S/PP-500, which substantially differs from other sulfured materials prepared from non-polymeric precursors, e.g., poly(S-r-DIB) [poly(sulfur-random-1,3-diisopropenylbenzene)].<sup>[34]</sup> Thus, although sulfur is covalently bound to poly(S-r-DIB), too, it can break up into low-molecular weight fragments during dis-

charge, resulting in a polysulfide shuttle. S/PP-500 based on a polymeric precursor does not form such fragments.

## Electrochemical performance of S/PP-500

Cyclic voltammetry (CV) was carried out in a voltage range between 0.45 V and 3 V (Figure 5a), in which the first discharge (black line) showed a broad signal that differed from the following CV curves. The first CV cycle was characterized by a broad reduction peak in the range of 0.6–1.8 V as well as a

weak oxidation peak at 1.7 V followed by a pronounced one at 2.3 V. This can be ascribed to the reduction of the polymer backbone, which is often observed in cathode materials with covalently bound sulfur.<sup>[21,23]</sup> By contrast, the following cycles showed one single reduction peak at 1.5 V and one oxidation peak at 2.4 V. These two signals shifted slightly during the first 20 cycles, suggesting that S/PP-500 experiences some structural changes up to the 20<sup>th</sup> cycle, probably related to changes in the average chain length of the C–S<sub>x</sub>–C moieties. Accordingly, different patterns for a pristine sample (black line, Figure 4a) and for one discharged and then fully recharged to 3 V (blue line, Figure 4a) were observed. Notably, again, no signals corresponding to the formation of long-chain polysulfide (ca. 2.3 V) were observed.<sup>[18]</sup>

The cutoff voltage is an important parameter in the characterization of new materials. Here, the classic voltage range from 1–3 V was not suitable for S/PP-500. As can be deduced from Figure 5ab, the reduction peak is not fully finished at 1 V (CV of S/PP-500 at various cycles with a voltage range of 1–3 V is shown in Figure S2). Incomplete cycling can result in poor electrochemical performance. As shown in Figure 5b, at the same condition the current density using a cutoff voltage of 0.45 V was much higher than for the same cathode with a cutoff voltage at 1 V.

Results of the cycling test of S/PP-500 based cathodes are depicted in Figure 5c. In line with results from CV, the discharge capacity initially dropped quickly but reached a stable state after 20 cycles. This drop-in discharge capacity is likely to be caused by the aforementioned changes in the structure of S/PP-500. Considering the fact that no signal for long-chain polysulfides was observed, part of the sulfur in the pristine state may switch to ‘inactive’ sulfur, which is still covalently

bound to the polymer matrix, however, does not participate in the redox process. In Figure 5d, the black line represents the discharge capacity of S/PP-500 at 0.5 C (1 C = 1672 mA/g). A discharge capacity of up to ca. 780 mAh/g<sub>sulfur</sub> remained after the initial decrease in capacity. After 1000 cycles at 0.5 C, the discharge capacity was ca. 640 mAh/g<sub>sulfur</sub>, which corresponds to only 0.018% capacity decay per cycle. At a higher C-rate of 1 C, the S/PP-500-based cathode still showed a decent discharge capacity of ca. 520 mAh/g<sub>sulfur</sub> at 1 C after 20 cycles and ca. 450 mAh/g<sub>sulfur</sub> after 1000 cycles at 1 C (capacity decay per cycle was ca. 0.013%). The Coulombic efficiency (CE) was close to 100%, which is in agreement with the ultra-stable and long cycle stability. The cycling test for a cathode with a mass loading of 1.5 mg/cm<sup>2</sup> is shown in Figure S3. Cathode materials with lower sulfur loading of 0.88 mg/cm<sup>2</sup> displayed a discharge capacity that was ca. 15% higher than the one of cathodes with higher mass loading, indicating that the thin coatings had a better coating quality.

The discharge profile of S/PP-500 (Figure 5e) shows a first irreversible discharge capacity of ca. 2100 mAh/g<sub>s</sub>, attributable to the reduction of the polymer backbone. No plateau representing long-chain polysulfide was observed, which matches the results from CV and explains the high Coulombic efficiency and stable electrochemical performance. Discharge capacities up to 1000 mAh/g<sub>sulfur</sub> at 0.1 C and 400 mAh/g<sub>sulfur</sub> at 4 C were observed (Figure 5f). Sulfurated activated carbon fibers (S/ACF) were used as active cathode material in reference cells (Figure S4). Compared to S/PP-500, S/ACF showed almost no discharge capacity, owing to the formation of lithium polysulfides that react with the carbonate-based electrolyte, resulting in decomposition and poor electrochemical performance.<sup>[27]</sup> This comparison underlines the advantages of

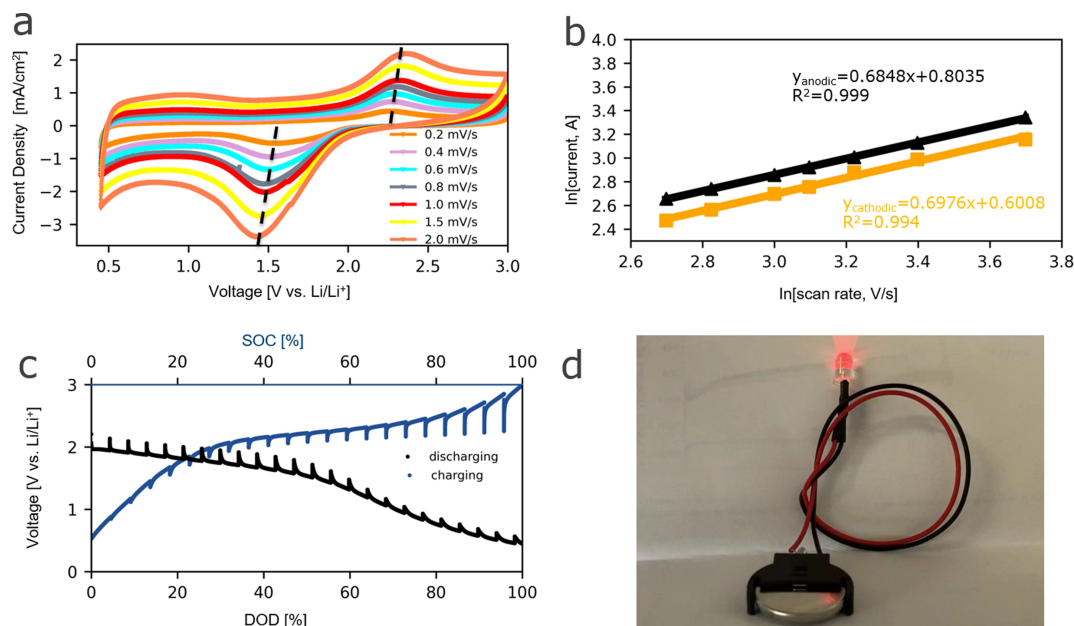


**Figure 6.** a) Cyclic voltammograms of S/PP-500 with a cutoff voltage at 0.5 V and scan rates between 0.2 and 2 mV/s. b) Double logarithmic plots of the current versus scan rate of S/PP-500. The cathodic peak is the yellow line, the anodic peak is the black line. c) GITT pulses applied for 10 min followed by 1 hour relaxation, 0.1 C, voltage range: 0.45–3 V. d) Image of an LED light bulb powered by an S/PP-500-based coin cell (anode: Li metal).

the S/PP-500 system. Indeed, only few types of cathode material (including SPAN)<sup>[21]</sup> are compatible with carbonate-based electrolytes.

Next, the kinetics of Li<sup>+</sup> insertion/extraction and the Li<sup>+</sup> diffusion rates were determined. CV was carried out at various scan rates between 0.2 and 2 mV/s. In addition, galvanostatic intermittent titration technique (GITT) was used. As shown in Figure 6a, with increasing scan rate (i.e., overpotential), the cathodic and anodic peaks shifted slightly towards a more negative and more positive potential, respectively. Moreover, the linear fit of the double logarithmic plot of the peak current vs. scan rate shown in Figure 6b yielded slopes of 0.6976 and 0.6848, respectively, which indicates a mixed mass transfer mechanism comprising both a diffusion-controlled and a surface absorption-controlled reaction.<sup>[36]</sup> Moreover, the lithium diffusion coefficients ( $D_{\text{Li, cathodic}} = 4.47 \times 10^{-9}$  and  $D_{\text{Li, anodic}} = 1.08 \times 10^{-8}$  cm<sup>2</sup>/s) were obtained using the Randles-Sevcik equation (Equation S1),<sup>[37]</sup> these are comparable to reported cathodes such as SPAN, SPANI or graphdiyne-like porous organic frameworks (Table S2).<sup>[28,38,39]</sup> Figure 6c shows a voltage curve for an S/PP-500 cathode material using the GITT technique. The curves display a pair of discharge and charge plateaus, which is in line with the discharge profile and strongly implies a solid phase reaction. Next, the diffusion coefficient of Li<sup>+</sup> at a given cutoff voltage was determined by the transient voltage response theory using the Weppner and Huggins equation (Equation S2). As can be seen in Figure S5, the lithium diffusion coefficient at 1 V as cutoff voltage was higher than at 3 V as cutoff voltage. This can be tentatively explained by the formation of Li<sub>2</sub>S<sub>2</sub>/Li<sub>2</sub>S at 0.45 V, which impeded the diffusion of Li<sup>+</sup> into the cathode. As mentioned above, the kinetic of this cell is partially controlled by diffusion. More Li<sub>2</sub>S<sub>2</sub>/Li<sub>2</sub>S formation blocks the ion diffusion, therefore the diffusion coefficient of cutoff voltage at 0.45 is lower, whereas the discharge capacity of cutoff voltage at 0.45 is much higher than cutoff voltage at 1 V.<sup>[40]</sup>

## Conclusion

In summary, we developed a new cathode material (S/PP-500) made from inexpensive polypropylene by a simple one-step vulcanization method. XPS, PXRD, ToF-SIMS, UV-vis, GITT and CV measurements indicate that all sulfur is covalently bound to the polymer matrix in form of C–S<sub>x</sub>–C bonds. Owing to this structure, only solid phase transition occur, which successfully avoids the problematic polysulfide shuttle. As a result, both the rate and cycle stability of Li–S batteries are enhanced. S/PP-500 delivers a high discharge capacity of up to 1000 mAh/g<sub>sulfur</sub> at 0.1 C. At 0.5 C, it delivers a discharge capacity of ca. 780 mAh/g<sub>sulfur</sub>. A low capacity loss of 0.018% per cycle as well as a Coulombic efficiency close to 100% were observed. Furthermore, the high sulfur loading of 68 wt% in S/PP-500 allows for a sulfur loading of 47 wt% in the final cathode. These properties make S/PP-500 a promising cathode material for Li–S batteries. Additionally, this strategy might well be extended to

other S/polymer composites with promising performance in Li–S batteries.

## Experimental Section

### Synthesis of S/PP-500

Isotactic PP (1.0 g, average  $M_w$  12000 g/mol, Sigma-Aldrich, Germany) was placed inside a high-temperature resistant quartz glass tube containing sulfur (ca. 20 g). The mixture was first heated in a high-temperature furnace (Nabertherm, Germany) to 150 °C under a stream of N<sub>2</sub> and held at that temperature for 8 h. Then, it was heated to 500 °C for 5 h. The obtained sulfurized PP (S/PP-500) was Soxhlet-extracted with toluene for 72 hours to remove excess sulfur. Afterward, it was dried under vacuum overnight. To achieve a more homogeneous particle size distribution, S/PP-500 was ground and sieved through a 63 μm mesh sieve.

### Cell Preparation

The active material was mixed with carbon black and poly(vinylidene fluoride) (PVDF) in a ratio of 70:15:15 (wt%) in *N*-methyl-2-pyrrolidone (NMP, active material:solvent = 1:10, wt/wt). The dispersion was coated on carbon-coated copper foil (280 mm × 11 μm, MTI corporation, Richmond CA, United States) with a wet thickness of 300 μm and then dried at 40 °C under vacuum for several hours. Then, it was transferred to an oven and dried at 60 °C overnight. Cathodes 12 mm in diameter were punched out with a cathode puncher. The average sulfur content was 0.88 mg/cm<sup>2</sup> per cathode, corresponding to 1.5 mAh/cm<sup>2</sup>.

Swagelok-type cells were applied for cell fabrication; cells were assembled in an Ar-filled glovebox. Lithium metal foils (Alfa) were punched out with a hollow punch 12 mm in diameter. A 1 M LiPF<sub>6</sub> solution in a mixture of ethylene carbonate (EC) and diethyl carbonate (DEC) (50:50, wt%, Sigma) was employed as electrolyte. Two Freudenberg separators (12.5 mm diameter) were placed between the anode and cathode. 100 μL of electrolyte was added onto each of the separators.

### Electrochemistry

Cycle stability tests were conducted on a BasyTech XCTS-LAB system at a constant temperature of 22 °C. Cells were cycled between 0.45–3 V or 1–3 V. The C-rate was set to 0.5 C and 1 C (1 C = 1672 mA/g = 1 mA cm<sup>2</sup>), respectively. Rate stability tests were also conducted on a BasyTech XCTS-LAB system starting with 0.5 C for 20 cycles to reach a rather stable stage, followed by 5 cycles at 0.1, 0.5, 1, 2, 4, 2, 1, 0.5, 0.1 C each. Finally, cells were run for another 20 cycles at 0.5 C. For CV measurements, a three-electrode Swagelok T-type cell and a Biologic VMP3 were used. Lithium foil was applied both as counter and reference electrodes, while the cathode material was used as the working electrode. The scanning rate was set to 1 mV/s and the cutoff voltage was set to 0.45 V and 1 V, respectively. The scan rates in CV (Figure 6a) were varied between 0.2 mV/s and 2 mV/s. GITT was performed by cycling the batteries first for 10 cycles at 0.5 C, followed by cycling at 0.1 C for 10 min (all between 0.45 V and 3 V), followed by 1 h relaxation.

Ex-situ XPS measurements were conducted on a Kratos Axis Ultra system using a monochromatic Al–K $\alpha$  source with a pass-energy of 20 eV for high-resolution measurements. The CasaXPS software was used for data analysis. A Shirley background was applied. For

the fitting of the spin-orbit split  $S\ 2p_{3/2}$  and  $S\ 2p_{1/2}$  peaks, the binding energy separation was set to 1.18 eV and the area ratios were constrained to 2:1.

X-ray powder diffraction (PXRD) was carried out on a Rigaku SmartLab using transmission geometry. Samples of the cathodes prior to and after cycling were prepared as drifted samples between two sealed sheets of Mylar® foil in an argon-filled glove-box. All diffraction patterns were recorded using monochromatic  $Cu-K_{\alpha 1}$  radiation. For phase analysis, the software PDXL 2<sup>[41]</sup> was used together with the PDF-2 database.<sup>[31]</sup> Additionally, the determined phases were compared to single-crystal data given in the *Inorganic Crystal Structure Database* ICS.<sup>[42]</sup>

Thermogravimetric Analysis (TGA) was carried out on a Q500 TGA (TA instruments) in a temperature range of 45 to 800 °C under  $N_2$  atmosphere applying a heating rate of 10 K/min.

Mass spectroscopy was carried out on a Netzsch QMS 403 C Aëolos® in a temperature range of 45–800 °C under  $N_2$  atmosphere applying a heating rate of 10 K/min.

Time of Flight Secondary Ion Mass Spectrometry (ToF-SIMS) was carried out on an IONTOF ToF-SIMS-NCS in negative polarity using  $Bi^{3+}$  with 30 keV in the spectrometry mode as analyses beam and Cs sputtering with 500 eV.

Ultraviolet-Visible (UV-vis) measurements were conducted on UV-1800 (Shimadzu).  $LiPF_6$  in a mixture of EC:DEC at a volume ratio of 1:1 was applied as reference. The battery was cycled 100 times and then stopped at a cutoff voltage of 0.45 V.

Infrared spectroscopy was conducted on an FT-IR Alpha spectroscope (Bruker)

Elemental analysis (EA) was conducted on Vario MicroCube (Elementar Analysensysteme GmbH). Measurements were taken at 1100 °C against the pestanal standard Thiram (Sigma-Aldrich) and sulfanilamide from Elementar.

Nitrogen adsorption measurements for determining the specific surface area and the pore size distribution were carried out at 77 K on a Quantachrome Instruments Autosorb iQ MP automatic volumetric instrument. Samples were degassed for 8 hours at 50 °C under vacuum. Specific surface areas were evaluated using the 11 Brunauer-Emmett-Teller (BET) model; pore size distributions were evaluated using the (slit/cylinder/sphere pores) QSDTF method.

## Acknowledgements

We gratefully acknowledge financial support provided by the German Federal Ministry of Economic Affairs and Energy (project number 03ETE003E). The authors thank U. Hageroth from the German Institutes of Textile and Fiber Research (DITF) Denkendorf for the recording of SEM measurement and Leonie Reinders for the TGA-MS measurement. The authors also thank B. Förtsch, Institute of Inorganic Chemistry, University of Stuttgart, for elemental analyses and Dr. F. Ziegler, Institute of Polymer Chemistry, University of Stuttgart, for BET measurements. Open Access funding enabled and organized by Projekt DEAL.

## Conflict of Interest

The authors declare no conflict of interest.

## Data Availability Statement

The data that support the findings of this study are available from the corresponding author upon reasonable request.

**Keywords:** cathode · lithium-sulfur battery · polypropylene · solid-phase transition · sulfurization

- [1] Z. Yang, J. Zhang, M. C. W. Kintner-Meyer, X. Lu, D. Choi, J. P. Lemmon, *J. Liu, Chem. Rev.* **2011**, *111*, 3577–3613.
- [2] B. Huang, Z. Pan, X. Su, L. An, *J. Power Sources* **2018**, *399*, 274–286.
- [3] Y.-X. Yin, S. Xin, Y.-G. Guo, L.-J. Wan, *Angew. Chem. Int. Ed.* **2013**, *52*, 13186–13200; *Angew. Chem.* **2013**, *125*, 13426–13441.
- [4] M. Wild, L. O’neill, T. Zhang, R. Purkayastha, G. Minton, M. Marinescu, G. Offer, *Energy Environ. Sci.* **2015**, *8*, 3477–3494.
- [5] S. S. Zhang, *Electrochim. Acta* **2012**, *70*, 344–348.
- [6] W. Ren, W. Ma, S. Zhang, B. Tang, *Energy Storage Mater.* **2019**, *23*, 707–732.
- [7] A. Manthiram, Y. Fu, S.-H. Chung, C. Zu, Y.-S. Su, *Chem. Rev.* **2014**, *114*, 11751–11787.
- [8] Y. V. Mikhaylik, J. R. Akridge, *J. Electrochem. Soc.* **2004**, *151*, A1969.
- [9] Y. Zheng, S. Zheng, H. Xue, H. Pang, *J. Mater. Chem. A* **2019**, *7*, 3469–3491.
- [10] S. Li, W. Zhang, J. Zheng, M. Lv, H. Song, L. Du, *Adv. Energy Mater.* **2021**, *11*, 2000779.
- [11] X. Ji, K. T. Lee, L. F. Nazar, *Nat. Mater.* **2009**, *8*, 500–506.
- [12] M. Li, P. Hu, X. Wang, Z. Niu, Q. Zhou, Q. Wang, M. Zhu, C. Guo, L. Zhang, J. Lu, J. Li, *Energy Technol.* **2019**, *7*, 1800898.
- [13] Z. Li, L. Yuan, Z. Yi, Y. Sun, Y. Liu, Y. Jiang, Y. Shen, Y. Xin, Z. Zhang, Y. Huang, *Adv. Energy Mater.* **2014**, *4*, 1301473.
- [14] H. Wang, Y. Yang, Y. Liang, J. T. Robinson, Y. Li, A. Jackson, Y. Cui, H. Dai, *Nano Lett.* **2011**, *11*, 2644–2647.
- [15] G. Zheng, Y. Yang, J. J. Cha, S. S. Hong, Y. Cui, *Nano Lett.* **2011**, *11*, 4462–4467.
- [16] G. Zhou, D.-W. Wang, F. Li, P.-X. Hou, L. Yin, C. Liu, G. Q. M. Lu, I. R. Gentle, H.-M. Cheng, *Energy Environ. Sci.* **2012**, *5*, 8901–8906.
- [17] X. Liang, C. Y. Kwok, F. Lodi-Marzano, Q. Pang, M. Cuisinier, H. Huang, C. J. Hart, D. Houtarde, K. Kaup, H. Sommer, T. Brezesinski, J. Janek, L. F. Nazar, *Adv. Energy Mater.* **2016**, *6*, 1501636.
- [18] Y. He, Z. Chang, S. Wu, H. Zhou, *J. Mater. Chem. A* **2018**, *6*, 6155–6182.
- [19] R. Fang, J. Xu, D.-W. Wang, *Energy Environ. Sci.* **2020**, *13*, 432–471.
- [20] H. Yang, J. Chen, J. Yang, J. Wang, *Angew. Chem. Int. Ed.* **2020**, *59* (19), 7306–7318.
- [21] S. Warneke, A. Hintennach, M. R. Buchmeiser, *J. Electrochem. Soc.* **2018**, *165*, A2093.
- [22] T. Leberherz, M. Frey, A. Hintennach, M. R. Buchmeiser, *RSC Adv.* **2019**, *9*, 7181–7188.
- [23] J. Fanous, M. Wegner, J. Grimminger, Ä. Andresen, M. R. Buchmeiser, *Chem. Mater.* **2011**, *23*, 5024–5028.
- [24] P. Wang, J. Kappler, B. Sievert, J. Häcker, K. Küster, U. Starke, F. Ziegler, M. R. Buchmeiser, *Electrochim. Acta* **2020**, *361*, 137024.
- [25] Q. Wu, W. Zhang, S. Li, W. Zhong, H. Zhu, Z. Zeng, C. Yu, S. Cheng, J. Xie, *ACS Appl. Mater. Interfaces* **2022**, *5*, 5212–5218.
- [26] B. Duan, W. Wang, A. Wang, K. Yuan, Z. Yu, H. Zhao, J. Qiu, Y. Yang, *J. Mater. Chem. A* **2013**, *1*, 13261–13267.
- [27] X. Li, M. Banis, A. Lushington, X. Yang, Q. Sun, Y. Zhao, C. Liu, Q. Li, B. Wang, W. Xiao, C. Wang, M. Li, J. Liang, R. Li, Y. Hu, L. Goncharova, H. Zhang, T.-K. Sham, X. Sun, *Nat. Commun.* **2018**, *9*, 4509.
- [28] Y. Yi, W. Huang, X. Tian, B. Fang, Z. Wu, S. Zheng, M. Li, H. Ma, *ACS Appl. Mater. Interfaces* **2021**, *13*, 59983–59992.
- [29] X. Han, G. Qing, J. Sun, T. Sun, *Angew. Chem. Int. Ed.* **2012**, *51*, 5147–5151; *Angew. Chem.* **2012**, *124*, 5237–5241.
- [30] J. Guo, J. Zhang, F. Jiang, S. Zhao, Q. Su, G. Du, *Electrochim. Acta* **2015**, *176*, 853–860.

- [31] PDF-2, Newtown Square, Pennsylvania (USA) 1998.
- [32] Y. Idemoto, J. W. Richardson Jr, N. Koura, S. Kohara, C.-K. Loong, *J. Phys. Chem. Solids* **1998**, *59*, 363–376.
- [33] Y. Bi, T. Wang, M. Liu, R. Du, W. Yang, Z. Liu, Z. Peng, Y. Liu, D. Wang, X. Sun, *RSC Adv.* **2016**, *6*, 19233–19237.
- [34] A. G. Simmonds, J. J. Griebel, J. Park, K. R. Kim, W. J. Chung, V. P. Oleshko, J. Kim, E. T. Kim, R. S. Glass, C. L. Soles, Y.-E. Sung, K. Char, J. Pyun, *ACS Macro Lett.* **2014**, *3*, 229–232.
- [35] B. Warren, J. Burwell, *J. Chem. Phys.* **1935**, *3*, 6–8.
- [36] A. K. Timbola, C. D. Souza, C. Soldi, M. G. Pizzolatti, A. Spinelli, *J. Appl. Electrochem.* **2007**, *37*, 617–624.
- [37] X. Tao, J. Wang, C. Liu, H. Wang, H. Yao, G. Zheng, Z. W. Seh, Q. Cai, W. Li, G. Zhou, *Nat. Commun.* **2016**, *7*, 1–9.
- [38] J. Wang, F. Lin, H. Jia, J. Yang, C. W. Monroe, Y. NuLi, *Angew. Chem. Int. Ed.* **2014**, *53*, 10099–10104; *Angew. Chem.* **2014**, *126*, 10263–10268.
- [39] J. Ma, G. Xu, Y. Li, C. Ge, X. Li, *Chem. Commun.* **2018**, *54*, 14093–14096.
- [40] S. Murugan, S. Niesen, J. Kappler, K. Küster, U. Starke, M. R. Buchmeiser, *Batteries & Supercaps* **2021**, *4*, 1636–1646.
- [41] P. 2, *The Rigaku Journal* **2012**, *28*, 29–30.
- [42] ICSD, *FIZ Karlsruhe (GER)*, accessed Feb 2022.

---

Manuscript received: June 21, 2022  
Revised manuscript received: July 6, 2022  
Accepted manuscript online: July 6, 2022  
Version of record online: July 27, 2022